Formylglycinamide Ribonucleotide Amidotransferase from *Thermotoga maritima:* Structural Insights into Complex Formation[†,‡]

Mariya Morar,[§] Aaron A. Hoskins,[||,⊥] JoAnne Stubbe,[||] and Steven E. Ealick*[,§]

Department of Chemistry and Chemical Biology, Cornell University, Ithaca, New York 14853, and Departments of Chemistry and Biology, Massachusetts Institute of Technology, Cambridge, Massachusetts 02139

Received February 26, 2008; Revised Manuscript Received May 16, 2008

ABSTRACT: In the fourth step of the purine biosynthetic pathway, formyl glycinamide ribonucleotide (FGAR) amidotransferase, also known as PurL, catalyzes the conversion of FGAR, ATP, and glutamine to formyl glycinamidine ribonucleotide (FGAM), ADP, P_i, and glutamate. Two forms of PurL have been characterized, large and small. Large PurL, present in most Gram-negative bacteria and eukaryotes, consists of a single polypeptide chain and contains three major domains: the N-terminal domain, the FGAM synthetase domain, and the glutaminase domain, with a putative ammonia channel located between the active sites of the latter two. Small PurL, present in Gram-positive bacteria and archaea, is structurally homologous to the FGAM synthetase domain of large PurL, and forms a complex with two additional gene products, PurQ and PurS. The structure of the PurS dimer is homologous with the N-terminal domain of large PurL, while PurQ, whose structure has not been reported, contains the glutaminase activity. In *Bacillus subtilis*, the formation of the PurLQS complex is dependent on glutamine and ADP and has been demonstrated by size-exclusion chromatography. In this work, a structure of the PurLQS complex from *Thermotoga maritima* is described revealing a 2:1:1 stoichiometry of PurS:Q:L, respectively. The conformational changes observed in TmPurL upon complex formation elucidate the mechanism of metabolite-mediated recruitment of PurQ and PurS. The flexibility of the PurS dimer is proposed to play a role in the activation of the complex and the formation of the ammonia channel. A potential path for the ammonia channel is identified.

Since the structural characterization of tryptophan synthase twenty years ago, many examples of multidomain enzymes containing multiple active sites spatially separated from each other have been reported (*1–3*). According to the working hypothesis, this organization improves catalytic efficiency and enables channeling of unstable intermediates, and the active sites of such enzymes communicate and thereby affect each other's catalytic activity. An analogous strategy is thought to be utilized by macromolecular assemblies (*4, 5*). However, mechanisms by which these communications occur between either separate domains or proteins and characteristics of the channels within the multidomain enzymes or protein complexes remain to be fully characterized; additionally for macromolecular assemblies, the mechanisms of complex formation require investigation.

One group of enzymes with multiple spatially separated active sites are glutamine amidotransferases, which are responsible for various amination reactions where ammonia is generated in one active site and channeled to another containing the acceptor molecule (*6*). Formylglycinamide ribonucleotide amidotransferase (FGAR-AT[1]) is part of the purine biosynthetic pathway and catalyzes the synthesis of formyl glycinamidine ribonucleotide (FGAM) from FGAR (*7, 8*). FGAR-AT, also known by its gene product name PurL, utilizes an ATP molecule for the activation of the FGAR amide moiety producing ADP and phosphate. The ammonia source in the reaction is a glutamine, which is converted to a glutamate (Scheme 1).

Two forms of PurL have been observed, known as large and small PurL. The large PurL is found in Gram-negative bacteria and eukaryotes. It consists of a single polypeptide chain 140 kDa in size. The structure of a large PurL from *Salmonella typhimurium* (StPurL) is known, and the domain organization of this protein has been described (*9*). StPurL contains three major domains, the N-terminal domain, the FGAM synthetase domain, and the C-terminal glutaminase

[†] This work was supported by NIH Grants GM73220 to S.E.E. and GM32191 to J.S. S.E.E. is indebted to the Lucille P. Markey Charitable Trust and the W.M. Keck Foundation. A.A.H. was supported by a NSF predoctoral fellowship.

[‡] The coordinates of the TmPurLQS structure have been deposited in the Protein Data Bank under accession number 3D54.

* To whom correspondence should be addressed at the Department of Chemistry and Chemical Biology, Cornell University, Ithaca, NY 14853. Tel: (607) 255-7961. Fax: (607) 255-1227. E-mail: see3@cornell.edu.

[§] Cornell University.

[||] Massachusetts Institute of Technology.

[⊥] Current address: Department of Biochemistry and Molecular Pharmacology, U. Massachusetts Medical School, Worcester, MA 01655.

[1] Abbreviations: FGAR, formylglycinamide ribonucleotide; FGAM, formylglycinamidine ribonucleotide; FGAR-AT, formylglycinamide ribonucleotide amidotransferase; Tm, *Thermotoga maritima*; Bs, *Bacillus subtilis;* St, *Salmonella typhimurium;* MWCO, molecular weight cutoff; HEPES, 4-(2-hydroxyethyl)-1-piperazineethanesulfonic acid; MPD, 2-methyl-2,4-pentanediol; TEV, tobacco etch virus; DDMP, difference distance matrix plot; rmsd, root-mean-square deviation; PEP, phosphoenol pyruvate; PK, pyruvate kinase.

10.1021/bi800329p CCC: $40.75
Published on Web 07/03/2008

Scheme 1

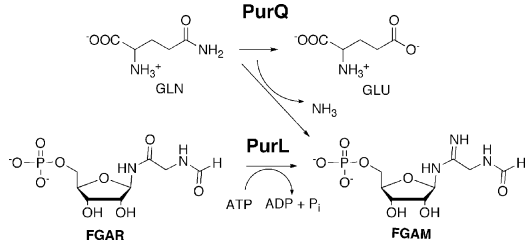

domain. The active site of the glutaminase domain is 45 Å away from the FGAM synthetase domain, and like all amidotransferases, it is believed that an ammonia channel connects the two active sites. Two paths for the ammonia channel have been proposed based on the StPurL structure.

Small PurL, found in Gram-positive and archaeal organisms, consists of a 60−80 kDa peptide chain, and is homologous to the FGAM synthetase domain of large PurL. Six structures of a small PurL from *Thermotoga maritima* have been described: that of the native enzyme (PDB entry 1VK3) and in complex with FGAR (PDB entry 2HS3), ATP (PDB entry 2HS0), AMPPCP (PDB entry 2HRY), ADP (PDB entry 2HRU), and FGAR and AMPPCP together (PDB entry 2HS4) (*10, 11*). Small PurL requires two additional gene products, PurQ and PurS, for glutamine-dependent activity. PurQ, 25 kDa in size, whose structure has not yet been reported, is the glutaminase responsible for the generation of ammonia. PurS has a mass of 10 kDa, and four structures of PurS from different organisms are available (PDB entries 1TWJ, 2CUW, 1VQ3, 1GTD) (*12–14*). These structures reveal the structural homology of the PurS dimer to the N-terminal domain of StPurL; nevertheless, the function of this protein remains to be elucidated.

PurL, PurQ and PurS must form a complex in order to generate FGAM with glutamine; however, the overall quaternary structure of the proteins in the complex requires confirmation (*12, 14*). In *Bacillus subtilis,* it was found that ADP and glutamine are necessary for the complex formation (*15*). Both large and small PurLs have one active site and one auxiliary site related by 2-fold pseudosymmetry, and in large PurLs, exemplified by the StPurL structure, the auxiliary site contains a structural $(Mg^{2+})_3$-ADP molecule (*9*). Consequently, it is the auxiliary site that is hypothesized to be important for the formation of the complex in small PurLs. However, the identity of the nucleotide binding in the auxiliary site and the mechanism by which it acts is unclear. In *B. subtilis* PurLQS, ADP was shown to be important, while the *T. maritima* PurL crystal structure contained a Mg^{2+}-ATP molecule bound in the auxiliary site and TmPurL was shown to bind ATP in solution (*11, 15*).

While the mechanism of ammonia production in the glutaminase domain is well-understood based on studies of homologous enzymes (*16*), less is known about FGAM synthesis (*17–19*). A sequential or a partially compulsory order mechanism for substrate binding has been reported for the FGAR-AT in various organisms, with Gln binding first followed by Mg-ATP and FGAR. However, the order by which the reaction proceeds or whether FGAR reacts with ATP or ammonia first is unclear, as is the order of product release (*17, 19*). The glutaminase activity has been shown to increase upon complex formation, yet the mechanism of this activation is unknown (*15*). The catalytic coupling between the active sites of PurQ and PurL as well as the role of PurS in this event requires further investigation. Although several structures of enzymes containing ammonia channels are known, no general properties for channels have yet been deduced based on these structures due to a large variability in their composition (*2*). The characteristics of the channel in PurLQS and the role of PurS in its formation are yet to be described.

In order to further characterize the FGAR-AT system and investigate the nature of protein interactions in the complex, coupling between the two active sites, and the formation and composition of the ammonia channel, a crystallographic study of PurLQS from *T. maritima* was undertaken. Comparisons of the TmPurLQS complex with the uncomplexed TmPurL and TmPurS as well as the StPurL structure resulted in observations of protein movements, attributed to the complex formation. These observations allowed for the description of a possible mechanism of communication between proteins within the complex and favored one of the two previously proposed ammonia channels.

EXPERIMENTAL PROCEDURES

Cloning of PurL, PurQ, and PurS from T. maritima. TmPurL and TmPurS genes were cloned by the Cornell Protein Characterization and Production Facility from genomic DNA using standard PCR procedures. The primers used for all constructs are listed in Supplemental Table 1 (Supporting Information). The first set of PCR products was used as template for another round of thermocycling with primers designed to add attB sites to the ends of the PCR products and insert a tobacco etch virus (TEV) protease recognition site at the N-terminus of the encoded protein. The resulting PCR products were purified and used in BP recombination reactions with the Invitrogen vector pDONR221 following the manufacturer's instructions. Correct clones were identified by PCR screening followed by sequencing. The correct clones were used in LR recombination reactions with the plasmid pDESTF1, which is a Gateway adapted vector based on the pET-system from Novagen. The plasmid pDESTF1 is under the control of the T7*lac* promoter and encodes an N-terminal 6xHis tag with the sequence MGSHHHHHHDITSLYKKAGS**ENLYFQ**HM (the TEV protease recognition site in bold). TmPurQ was cloned from genomic DNA and ligated into the *Nde*I/*Bam*HI sites of the pET-28a expression vector (Novagen). TmPurQ contained a polyhistidine tag at the N-terminus with the sequence MGSSHHHHHHSSG**LVPRGS**HM (thrombin recognition site in bold).

Expression and Purification of TmPurL, TmPurQ, and TmPurS. Three sets of *Escherichia coli* BL21(DE3) cells were each transformed with a plasmid containing one of the three protein constructs. Single colonies were used to inoculate 5 mL starter cultures in LB media, which were then grown overnight at 37 °C. Each starter culture was transferred into 1 L of LB media containing either kanamycin (40 μg/mL) for TmPurQ or ampicillin (100 μg/mL) for TmPurS and TmPurL, respectively. The cells were grown at 37 °C until $OD_{600\ nm}$ 0.4 was reached. The temperature was then reduced to 15 °C and, after 40 min of cooling, the cells were induced with 100 μM isopropyl β-D-thiogalactopyranoside for 12 h at OD_{600nm} 0.6. The cells were then

harvested via centrifugation at 9000*g* for 10 min at 4 °C using an Avanti J-25I centrifuge (Beckman) and stored at −20 °C. The typical yield was 5 g of cells per 1 L of culture.

The three proteins were purified following the same procedure at 4 °C. The cell pellet (5 g) was resuspended in 30 mL of lysis buffer, 100 mM Na_2HPO_4 (pH 8.0) and 300 mM NaCl. The cells were lysed via three passes through a French pressure cell press (SIM AMINCO Spectronic Instruments). The cell debris was removed via centrifugation at 35000*g* for 30 min. The cleared cell lysate was loaded at 1 mL/min onto a 2 mL Ni-NTA affinity agarose column (Qiagen) equilibrated with the lysis buffer. After the lysate was loaded, the column was washed with 100 mL of wash buffer, which consisted of the lysis buffer and 10 mM imidazole. The protein was eluted with an elution buffer, which was the lysis buffer with addition of 250 mM imidazole (pH 8.0). The protein elution was monitored by measuring protein concentration via Coomassie Plus Protein Assay Reagent (Pierce).

To remove the N-terminal polyhistidine tag, TmPurQ was incubated with thrombin, while TmPurS was incubated with TEV protease. The tag was not removed from TmPurL. Thrombin (10 U; BD Biosciences) was used per 1 mg of TmPurQ. The mixture was incubated in dialysis tubing (Pierce) with a 10 kDa molecular weight cutoff (MWCO) (Millipore) for 12 h at 4 °C in a buffer that was 50 mM Tris (pH 8.5), 300 mM NaCl, 2 mM dithiothreitol, 2 mM $CaCl_2$, 2 mM $MgCl_2$, and 2% glycerol. The digestion of TmPurS in thrombin digestion buffer with TEV protease was also performed via dialysis at 4 °C for 36 h. TEV protease was provided by the Cornell Protein Production Facility. Following the digestion each protein solution was loaded onto a Ni-NTA column for the second time and the flow-through was retained.

All three proteins were further purified by gel filtration chromatography. A Hi-Load Superdex 75 column (26/60, Amersham) was equilibrated with 50 mM Tris buffer (pH 8.5), 300 mM NaCl, 10 mM KCl, 10 mM $MgCl_2$, and 2 mM L-glutamine. Each of the three proteins was eluted separately at a flow rate of 1 mL/min while monitoring the A_{280nm} and collecting 2 mL fractions. The fractions containing the protein as evidenced by SDS gel analysis were combined and concentrated to 10 mg/mL using an Amicon Ultra centrifugal device with a 10 kDa MWCO (Millipore). The purity of the proteins was assessed by SDS gel analysis (data not shown).

Activity Assays. The TmPurLQS complex was reconstituted in 50 mM HEPES (pH 7.2), 20 mM KCl, and 20 mM $MgCl_2$ by ordered addition of 200 μM TmPurS, 100 μM TmPurQ, and 100 μM TmPurL. The complex was allowed to sit on ice for 5 min before assaying. Assays were carried out as previously described (*2*) at 37 °C in 50 mM HEPES (pH 7.2), 20 mM KCl, 20 mM $MgCl_2$, 10 mM ATP, 1 mM β-FGAR, 20 mM L-glutamine, and 2 U/mL of histag-*E. coli* PurM as the coupling enzyme. In some experiments, the buffer was depleted of ADP by addition of 3 mM phosphoenolpyruvate (PEP) and 10 U/mL pyruvate kinase (PK, 451 U/mg, Sigma) before addition of TmPurLQS. The TmPurLQS complex was then assayed at concentrations of 1−5 μM, and FGAM synthesis was monitored using the modified Bratton−Marshall assay.

Table 1: Summary of Data Collection and Processing Statistics[a]

	TmPurLQS
resolution (Å)	50−3.5
no. of reflections	392757
no. of unique reflections	93030
I/σ	12.0 (2.1)
completeness	99.7 (99.1)
R_{sym}[b]	12.6 (52.6)
redundancy	4.2 (3.9)

[a] Values for the highest resolution shell are given in parentheses. [b] $R_{sym} = \sum\sum_i |I_i - \langle I \rangle| / \sum \langle I \rangle$, where $\langle I \rangle$ is the mean intensity of the N reflections with intensities I_i and common indices h,k,l.

Complex Reconstitution and Crystallization. The TmPurLQS complex was reconstituted by combining the three proteins in a 1:1:2 ratio of TmPurL:TmPurQ:TmPurS, respectively, in their purification buffers, followed by addition of 5 mM ATP and 5 mM ADP. The purification buffers contained 2 mM glutamine, which was necessary for complex formation. The mixture was incubated at 4 °C for 30 min. Gel filtration chromatography was then performed on the TmPurLQS complex as described above using the same purification buffer as for the individual proteins. The fractions containing all three proteins were combined and concentrated to 20 mg/mL. This solution was used for crystallization experiments and stored at −80 °C when not used.

Sparse matrix screens from Wizard and Hampton were used to obtain the initial crystallization conditions. The hanging drop vapor diffusion method was used with 1 μL of protein being combined with 1 μL of well solution. The initial crystallization conditions were further improved via the Hampton additive screen. The optimized crystallization condition contained 55% MPD, 0.1 M HEPES (pH 7.5), and 7% xylitol. Crystals grew in 2 weeks at 18 °C. For data collection, the crystals were frozen in liquid nitrogen by direct transfer from the mother liquor. TmPurLQS crystallizes in the monoclinic space group *C*2 with three molecules per asymmetric unit, 78% solvent content, and cell dimensions of $a = 256.9$ Å, $b = 187.3$ Å, $c = 159.2$ Å, $\beta = 99.1°$. The crystals diffract to 3.5 Å resolution.

Data Collection and Processing. The data were collected at the NE-CAT 24-ID-C beamline of the Advanced Photon Source at Argonne National Laboratory (Argonne, IL). A Quantum 315 detector (Area Detector Systems Corp.), 1 s exposure time, 1° oscillation step, and 300 mm crystal to detector distance were used to record diffraction images. The HKL2000 program suite (*20*) was used for indexing, integration and scaling of the data. Data processing statistics are summarized in Table 1.

Structure Determination and Refinement. The structure of the TmPurLQS complex was determined by molecular replacement using the program Phaser from the CCP4 (*21*) interface to calculate the rotation and translation functions at 5 Å resolution. Two models were used simultaneously for the calculations; the first model was the native TmPurL structure (PDB entry 1VK3); the second search model was that of PurLQS constructed based on the StPurL structure (PDB entry 1T3T). In the second model, the domain organization of the StPurL structure was used to position TmPurL and the TmPurS dimer (PDB entry 1VQ3), via superposition with the FGAM synthetase and the N-terminal domains, respectively. The glutaminase domain of StPurL was used as the search model for TmPurQ since they have

Table 2: Refinement Statistics

	TmPurLQS
total no of non-hydrogen atoms	22659
no. of protein atoms	22548
no. of ligand atoms	111
no. of reflections in refinement	78498
no. of reflections in test set	7909
R^a	25.5
$R_{free}{}^b$	28.4
rmsd bond (Å)	0.009
rmsd angle (deg)	1.2
average *B* factor (Å^2)	137.0
Wilson *B* factor (Å^2)	88.6
Ramachandran plot:	
most favored (%)	81.8
additionally allowed (%)	17.0
generously allowed (%)	0.7
disallowed (%)	0.5

[a] R factor $= \sum_{hkl}||F_{obs}| - k|F_{calc}||/\sum_{hkl}|F_{obs}|$, where F_{obs} and F_{calc} are observed and calculated structure factors, respectively. [b] In R_{free} the sum is extended over a subset of reflections that were excluded from all stages of refinement.

35% sequence identity. Three molecules of TmPurLQS were positioned in the asymmetric unit with the following Phaser statistics: rotation function *Z*-scores of 8.6, 9.2, and 4.8, translation function *Z*-scores of 8.4, 21.7, and 18.1, and log-likelihood gain scores of 156, 518, and 700.

Refinement of the model was done using CNS (*22*). Rounds of rigid body refinement, annealing, *B* factor refinement, and minimization were performed followed by manual model building in COOT (*23*). Throughout the refinement tight noncrystallographic symmetry restraints (NCS) were used. The averaging of the maps was done using RAVE (*24*). The averaged composite omit electron density map was used when building the model manually. The averaged $F_o - F_c$ difference map was used to position two ligands: an ADP bound in the auxiliary site of TmPurL, and a glutamyl thioester intermediate covalently linked to Cys86 of TmPurQ. Final refinement statistics are summarized in Table 2.

Figure Preparation. All figures were prepared using ChemDraw and PyMOL (*25*).

RESULTS

Activity and Crystallization of the TmPurLQS Complex. TmPurL, TmPurQ, and TmPurS were individually expressed in *E. coli* and purified with the use of N-terminal polyhistidine tags. After reconstitution of the tagged TmPurLQS complex, glutamine-dependent FGAM synthesis could be observed with a specific activity of 0.016 μmol/min/mg at 37 °C. The presence of protease recognition sites in the polyhistidine tags afforded the opportunity to remove the tags and prepare wild type TmPurQ and TmPurS, while the preparation of wild type TmPurL has been previously described (*11*). After tag removal, the activity of the reconstituted, wild type TmPurLQS complex rose to 0.031 μmol/min/mg at 37 °C. This activity is substantially lower than that observed for either StPurL (4.4 μmol/min/mg) or *B. subtilis* PurLQS (BsPurLQS) (1.3 μmol/min/mg) under similar conditions (*15, 26*). In addition, this activity is lower than the NH_3-dependent activity of TmPurL at 37 °C (0.3 μmol/min/mg) (*11*). This suggests that the thermophilic complex may not be functioning optimally at 37 °C and a more detailed kinetic analysis is warranted at a physiologically relevant temperature.

Interestingly, if the assay buffer was depleted of ADP by the addition of PK/PEP, the activity of the reconstituted complex remained the same (0.038 μmol/min/mg). This suggests that if ADP is required for complex formation as observed for BsPurLQS (*15*), ADP could be generated from ATP by TmPurLQS and/or the complex is more efficient at scavenging ADP than PK/PEP. Alternatively, ADP and ATP could be functionally equivalent for complex formation for TmPurLQS. These observations are noteworthy in light of the structural description of the TmPurL auxiliary site discussed below.

For crystallization, the tagged TmPurL was used; however, it was necessary to remove the tags from TmPurS and TmPurQ, as they interfered with crystal growth. Moreover, it was necessary to preform the complex in the presence of glutamine and ADP/ATP, followed by isolation via size-exclusion chromatography. The formation of the complex was evident from the TmPurLQS elution profile, which had a shorter retention time than TmPurL by itself. Based on a standard molecular mass calibration curve for the given column, the complex eluted at a volume consistent with an 80 kDa apparent molecular mass. Previous studies of PurS from various organisms have shown that this protein is unlikely to exist as a monomer eliminating the possibility of a 1:1:1 complex (*12–14*). Therefore our observation is indicative of a (2 TmPurS):(1 TmPurQ):(1 TmPurL) stoichiometry (predicted 109 kDa) and rules out a 4:2:2 complex (218 kDa, Supplemental Figure 1, Supporting Information). Under these conditions, complex formation was not complete as evident from the elution chromatogram and SDS gel analysis. Isolation of the complex prior to crystallization to remove uncomplexed proteins proved essential to determination of the structure.

Quality Assessment of the Final Model. The final model contains three proteins complexed together, TmPurL, TmPurQ, and a dimer of TmPurS. TmPurL is a 63 kDa protein, and contains a total of 603 residues. The model of TmPurL is missing residues 186−203, a large loop which becomes ordered upon FGAR binding (*11*). TmPurQ has a molecular mass of 23.6 kDa and 213 residues, all of which were present in the final model. Two molecules of TmPurS, 9.6 kDa and 82 residues each, are present as a dimer. All of the TmPurS residues were included in the final model. The final *R* factor was 25%, and the R_{free} value was 28%. The quality of the model was validated using PROCHECK (*27*).

Overall Organization of the TmPurLQS Complex. TmPurL, TmPurQ, and TmPurS form a complex with the stoichiometry of 1:1:2, respectively. The complex has a globular shape with the dimensions of 90 × 85 × 75 Å^3, and the total surface area of 34,300 Å^2 (Figure 1). Each of the three proteins interacts with the other two, and a small part of the interface is common to all three proteins. Half of the TmPurQ surface area is involved in the complex formation, while for TmPurS and TmPurL, the surface area at the interface comprises 35% and 20% of the total, respectively. The largest protein interface is formed between TmPurL and TmPurQ, with a surface area of 2,800 Å^2. The interface area between TmPurL and TmPurS is 1,400 Å^2, and that between TmPurS and TmPurQ is 2,000 Å^2.

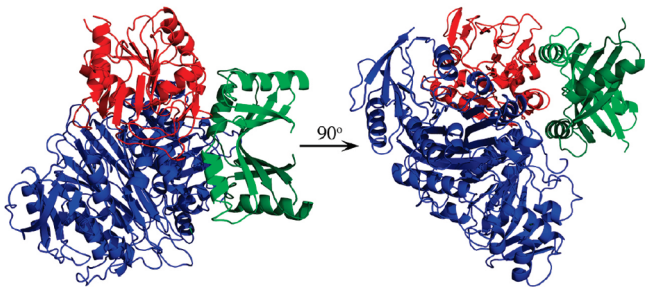

FIGURE 1: Overall structure of the TmPurLQS complex. TmPurL is in blue; TmPurQ is in red; the TmPurS dimer is in green.

TmPurQ. The structure of TmPurQ reported herein is the first among the PurQ enzymes. TmPurQ contains a classic triad glutaminase fold; it consists of a nine stranded mixed β-sheet flanked by four helices, a pair of strands, and four 3_{10} helices (Figures 2A and 2B). The active site is composed of four loops, located between β3 and α2, β4 and α4, β7 and β8, and β11 and α5. In the complex structure, the TmPurQ active site is occupied by a glutamyl thioester intermediate covalently bound to Cys86 (Figure 2C). N4 of the His186 imidazole ring, most likely protonated, is positioned to transfer the proton to the Cys86 sulfur upon hydrolysis of the thioester moiety. In turn, the N2 of His186 forms a hydrogen bond with the side chain of Glu188. These three residues form the catalytic triad and are strictly conserved among all PurQs. Moreover, comparison with other triad glutaminases whose structures have been reported reveals structural conservation in the orientation and geometry as well as in the hydrogen bonding network of the triad residues (*9, 28–30*). Gly50, Phe51, Ala141, and Phe144 are positioned to form hydrogen bonds with the glutamyl moiety of the reaction intermediate via backbone atoms. All of these residues with the exception of Phe144 are strictly conserved among PurQ enzymes.

TmPurS. The structure of TmPurS has been reported (*14*). The monomer of TmPurS consists of a three-stranded antiparallel β-sheet, which is flanked by two helices (Supplemental Figure 2, Supporting Information). The biological unit of TmPurS is a dimer with the two monomers coming together to form a six-stranded β-sheet.

TmPurL. The structure of TmPurL has been described previously (*10, 11*). The enzyme consists of four subdomains, labeled as A1, A2, B1, B2 in Figure 3A. Subdomains A1 and A2 make up the central β-barrel, while subdomains B1 and B2 flank the barrel. The active site is located in the cleft between A1 and B1.

The auxiliary site, thought to be important for complex formation, is located in the cleft between subdomains A2 and B2 (*15*). As expected, the auxiliary site of the complexed structure contains a nucleotide (Figure 3B). The low resolution of the structure and the quality of the electron density observed for the nucleotide made its identification challenging. The density was modeled as an ADP molecule; however, the possibility of an ATP molecule with a disordered γ-phosphate cannot be ruled out.

The adenine moiety of the nucleotide is positioned to form two hydrogen bonds with Asp107 via N1 and N6. The 3′-hydroxyl of the ribose moiety donates a hydrogen bond to the carbonyl of Gly388. The α-phosphate of ADP interacts with Arg139, while the β-phosphate interacts with Ser548 and Lys429. The auxiliary nucleotide in TmPurLQS binds in a nearly identical orientation and geometry as the auxiliary ATP in the reported TmPurL structure (*11*), and all of the above listed interactions are conserved between the two structures.

Protein Interactions, Interface between TmPurS and TmPurL. In the TmPurLQS complex most of the protein−protein interactions are mediated via loops. The smallest of the interfaces is that between TmPurL and TmPurS. Here, one monomer from the TmPurS dimer contributes residues 12−26, which are located in the loop between β1 and α1, and residues 71−74 found between α2 and β3 (Figure 4A). Subdomains A1 and B1 from TmPurL come in contact with TmPurS via four major loop regions. One loop, between α4 and α5, consisting of residues 78−82, comes from the A1 subdomain; the remaining three loops, located between β5 and α7 (residues 180−185), α7 and α8 (residues 203−213), and α11 and β9 (residues 305−307), come from subdomain B1. The interface consists of four hydrogen bonds listed in Supplemental Table 2 (Supporting Information) and a hydrophobic patch formed by residues Tyr12, Val16, Val73, Val74 from TmPurS and Ile78, Ile207, and Val209 from TmPurL.

Protein Interactions, Interface between TmPurS and TmPurQ. Both monomers of the TmPurS dimer interact with TmPurQ via three main regions (Figure 4B). One monomer contributes α1, while the other contributes two loops found between β1 and α1 and between α2 and β3. TmPurQ interacts with TmPurS via loops in three regions. The first region is found between β3 and α3, includes residues 53−67, and involves a 3_{10} helix, α2, and the loops associated with these secondary structural elements. The second region is composed of residues 93 to 109, which is mostly a large loop that includes the C-terminal end of α4, and all of β5. The third region consists of β8 and the loops associated with this strand.

The TmPurS/Q interface buries a similar number of hydrophobic and hydrophilic residues. There are two hydrogen-bonding networks found in this interface with the major interactions listed in Supplemental Table 2. Two hydrophobic patches are present; one includes residues Ile24, Val27, and Val62 from one PurS monomer, residues Leu68 and Leu69 from the second PurS monomer, and residues Tyr53, Leu57, and Val62 from TmPurQ. The second hydrophobic patch is made up of residues Tyr12, Val16, Val73 and Val74 from the second PurS monomer and Ala101, Leu103, Ile93, Val148, and Ile150 from TmPurQ.

Protein Interactions, Interface between TmPurL and TmPurQ. The largest protein interface is formed between TmPurL and TmPurQ with most of the interactions mediated through loops (Figure 4C). All four subdomains from TmPurL are involved in the interface formation through six regions: helix α6 (residues 116−130) from subdomain A1, the loop preceding helix α8 (residues 211−220) from subdomain B1, the long connector loop between α12 of subdomain B1 and β12 of subdomain A2, β12 itself, and last the connector loop between β16 of A2 and β17 of B2 (residues 504−509). Most of the contribution comes from the central β-barrel, and less from the flanking subdomains.

TmPurQ contributes five regions consisting of loops and helices to the TmPurL/Q interface. These include the turn between β1 and α1 and the helix itself (residues 9−25), the 3_{10} helix including residues 50−56, the loop between β5 and

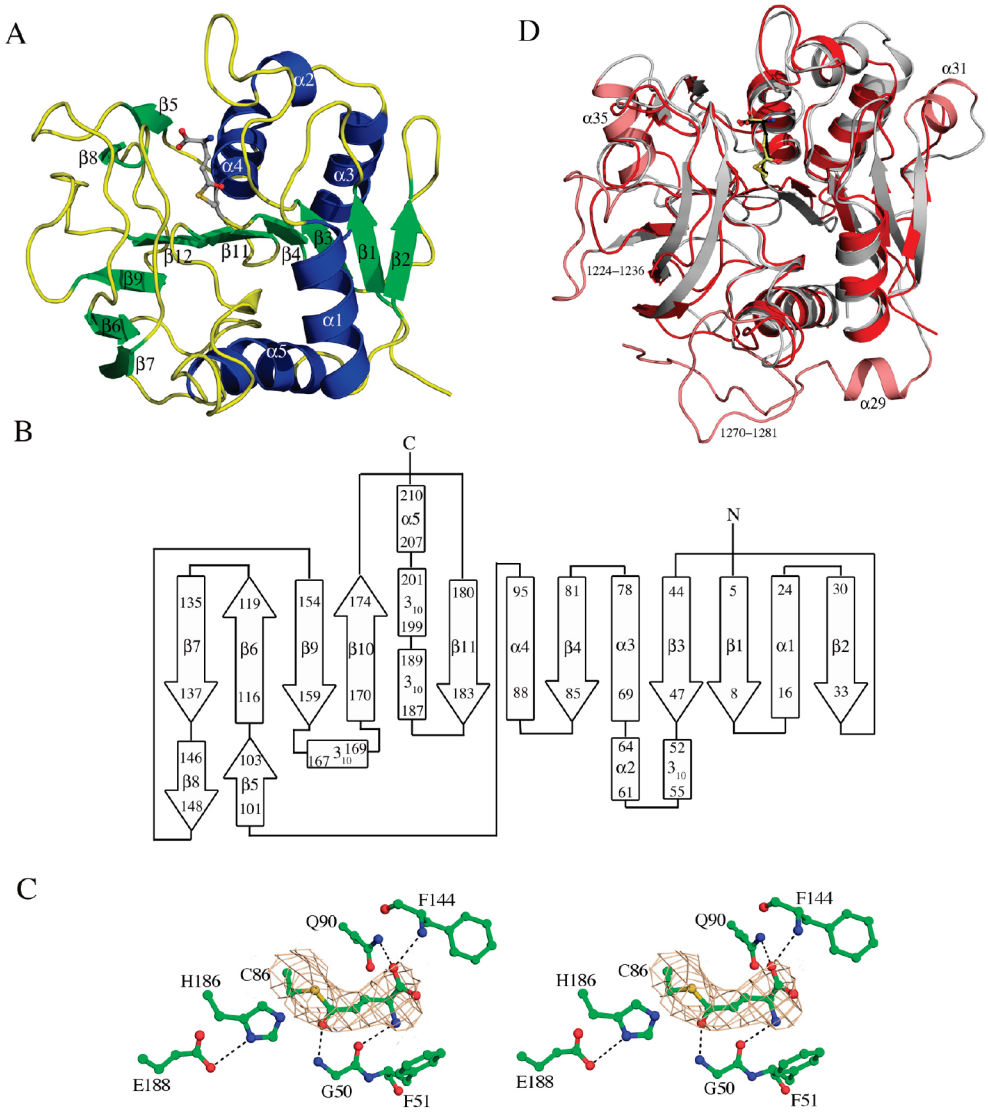

FIGURE 2: Structure of TmPurQ. (A) A ribbon diagram of the overall structure of TmPurQ. In blue are α-helices, in green are β-strands, in yellow are loops. In gray is ball-and-stick representation of the glutamyl thioester intermediate bound to Cys86. (B) The topology diagram of TmPurQ. (C) Stereoview of the active site of TmPurQ. The glutamyl thioester intermediate and the residues interacting with it are shown in ball-and-stick representation, colored green. Hydrogen bonds are shown as dotted lines. The NCS averaged composite omit $2F_o - F_c$ electron density for the ligand is shown at a contour level of 1σ and colored salmon. (D) Comparison of the complexed TmPurQ structure with the glutaminase domain of StPurL. A ribbon diagram of the superposition of TmPurQ, in red, with the glutaminase domain of StPurL, in gray. In salmon are the insertions of the glutaminase domain of StPurL. In ball-and-stick representation is the glutamyl thioester intermediate bound at the active site.

β6 (residues 109−114), the loop between β7 and β8 (residues 137−141), and the loop between the two 3_{10} helices at the C-terminus (residues 189−196).

This interface is mostly packed with polar and charged residues, which form approximately ten hydrogen bonds (Supplemental Table 2). Two small hydrophobic patches are found at the TmPurL/Q interface. One consists of Val382 and Val507 from TmPurL and Leu119, and Ile195 of TmPurQ. The second cluster is rich in aromatic residues with Phe213, Met217 and Leu305 from TmPurL, and Pro11, Tyr53, and Tyr56 from TmPurQ. Two phenylalanine residues from TmPurQ, Phe51 and Phe110, proposed to be the entrance of the ammonia channel and located in first shell of the TmPurQ active site, are also found at this interface.

Interface Common to All Three Proteins. A small part of the complex interface involves all three proteins (Figure 4D, surface area of 230 Å^2). Helix α1 of monomer 1 spans between TmPurL and TmPurQ with the central residues, Pro19, Arg20, and Thr23, contacting both domains. The carbonyl moiety of Pro19 is positioned to make hydrogen bonds with the amide and the side chain hydroxyl of Thr23. For TmPurQ, the 3_{10} helix located between β3 and α2 contributes Tyr53 and Tyr56, and TmPurL contributes residues 211−213 in a loop located between α7 and α8. Asp211 is near the hydroxyl moiety of Tyr56 in TmPurQ, while Phe213 is part of the hydrophobic interaction with Tyr53 and Tyr56 of TmPurQ.

DISCUSSION

Reliability of the 3.5 Å Structure. The structure of the TmPurLQS complex was determined at 3.5 Å resolution. While structures at this resolution are often prone to large errors and possible misinterpretation, TmPurLQS represents a favorable case. The structures of TmPurL and TmPurS were available at higher resolution and many homologous

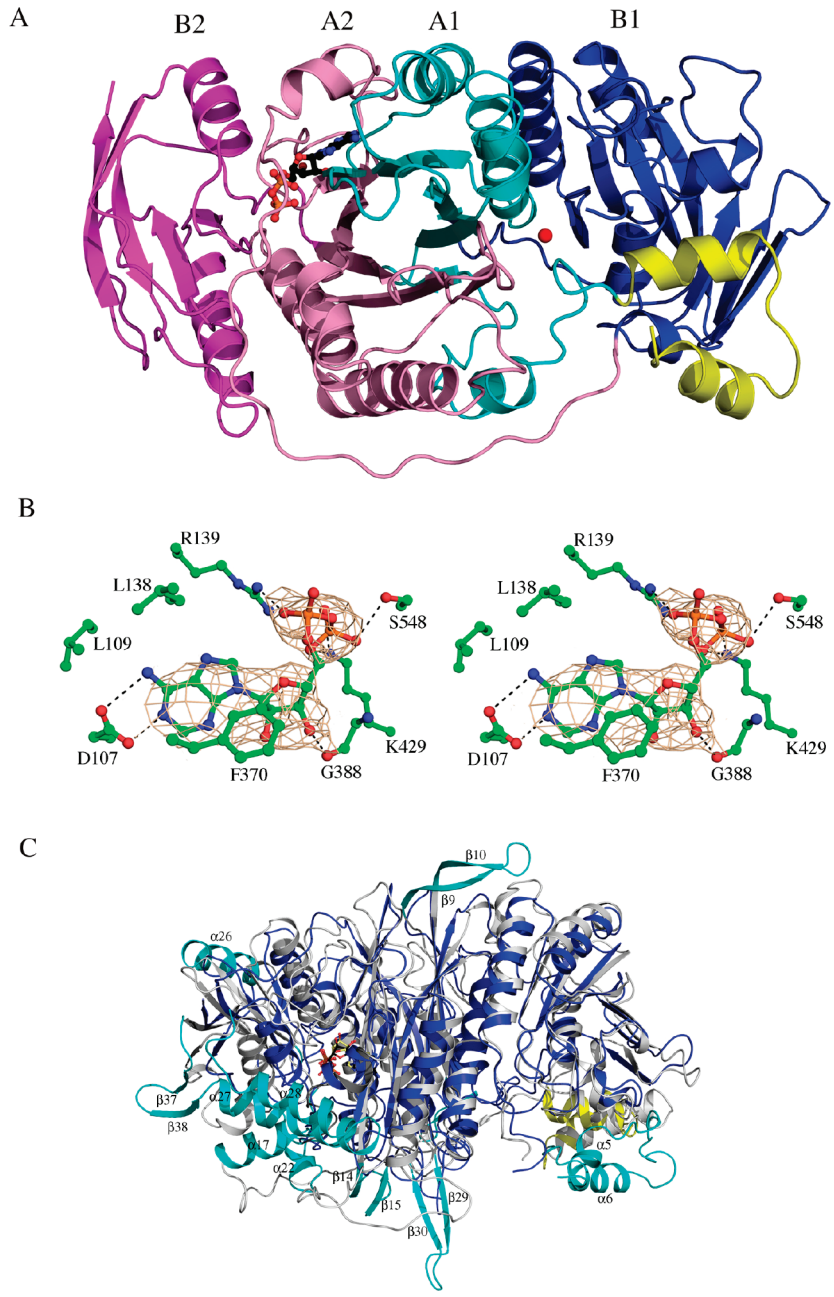

FIGURE 3: The structure of TmPurL. (A) A ribbon diagram of TmPurL. Subdomains A1, A2, B1, and B2 are colored cyan, pink, blue, and magenta, respectively. In yellow are the linker helices. In ball-and-stick representation is the ADP molecule bound in the auxiliary site. The red sphere is the Na^+ atom bound in the active site. (B) Ball-and-stick representation of the auxiliary site of TmPurL. Hydrogen bonds are shown as dotted lines. The NCS averaged composite omit $2F_o - F_c$ electron density for the ligand is shown at a contour level of 1σ and colored salmon. (C) Comparison of the complexed TmPurL structure with the FGAM synthetase domain of StPurL. A ribbon diagram of the superposition of TmPurL, in blue and with the FGAM synthetase domain of StPurL, in gray. The linker of TmPurL is in yellow; in cyan are the insertions of the FGAM synthetase domain of StPurL.

triad glutaminase structures are available, thus making both the backbone and side chains of the initial model more reliable. In addition the asymmetric unit contains three complete complexes, allowing for NCS map averaging during model building and NCS restraints during refinement. The effect of tight NCS restraints are reflected in only a 4% difference in the *R*-factor and *R*-free. Finally, tight geometrical constraints were maintained throughout the refinement process. As a result the 3.5 Å structure of TmPurLQS is accurate enough to infer hydrogen bonds for most regions of the structure.

Comparison of the Organization of the TmPurLQS Complex with StPurL. The protein organization in the TmPurLQS complex is very similar to the domain organization in StPurL. The overall root-mean-square deviation (rmsd) for the Cα carbon backbone for the two structures is 2.8 Å^2. StPurL is larger than TmPurLQS with a surface area of 41,000 Å^2, compared to 34,300 Å^2 for the complex. The domains of StPurL bury about 10% of the surface area of all three domains, while for TmPurLQS, 9% is buried. In StPurL, the FGAM synthetase domain forms larger interfaces with the glutaminase and the N-terminal domains, burying 4,700 Å^2 and 1,900 Å^2, respectively, compared to 2,800 Å^2 and 1,400 Å^2 for TmPurLQS. However, the interface between the glutaminase domain and the N-terminal domain of StPurL

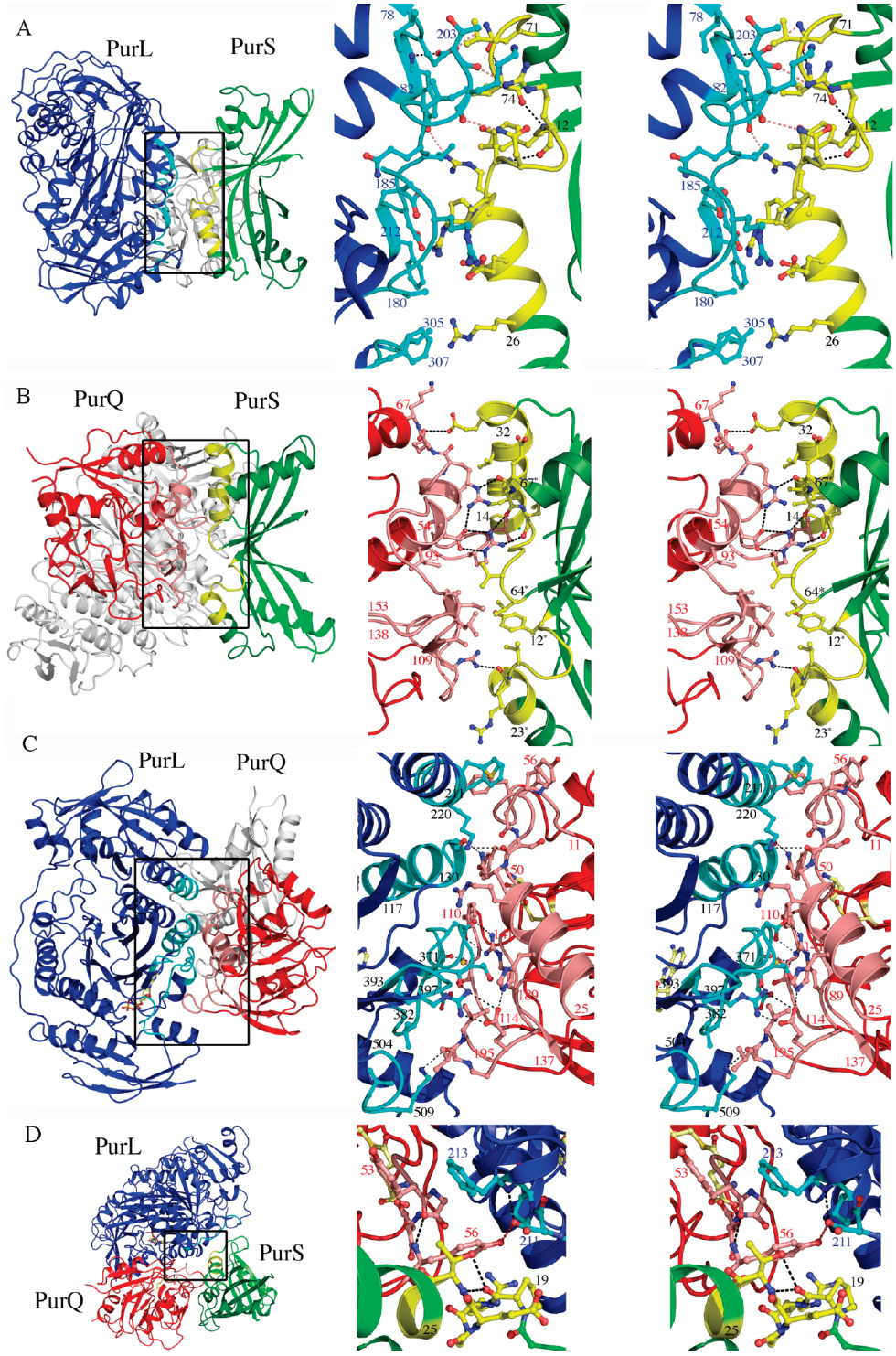

FIGURE 4: Protein−protein interfaces of the TmPurLQS complex. (A) A ribbon diagram of the TmPurL/S interface. TmPurL is in blue; TmPurS is in green. The structural elements involved in the interface formation are in cyan, and in yellow for TmPurL and TmPurS, respectively. In ball-and-stick representation are the residues located directly at the interface. Dotted lines are hydrogen bonds. (B) A ribbon diagram of the TmPurQ/S interface. TmPurQ is in red; TmPurS is in green. The structural elements involved in the interface formation are in salmon, and in yellow for TmPurQ and TmPurS, respectively. (C) A ribbon diagram of the TmPurL/Q interface. TmPurL is in blue; TmPurQ is in red. The structural elements involved in the interface formation are in cyan, and in salmon for TmPurL and TmPurQ, respectively. (D) A ribbon diagram of the TmPurL/Q/S interface. TmPurL is in blue, TmPurQ is in red; and TmPurS is in green. The structural elements involved in the interface formation are in cyan, salmon, and yellow for TmPurL, TmPurQ and TmPurS, respectively. In ball-and-stick representation are the residues located directly at the interface.

buries 1,800 Å^2, which is comparable to the TmPurQ/S interface (2,000 Å^2).

Comparison of TmPurQ with the Glutaminase Domain of StPurL. The glutaminase domain of StPurL shares 35% sequence identity with TmPurQ. The two structures have an rmsd of 1.7 Å^2, and the core glutaminase fold of TmPurQ superimposes well with the glutaminase domain of StPurL (Figure 2D). The difference between the two structures consists of three alpha helices, α29, α31, α35, and two loops, present in the glutaminase domain of StPurL, and absent in

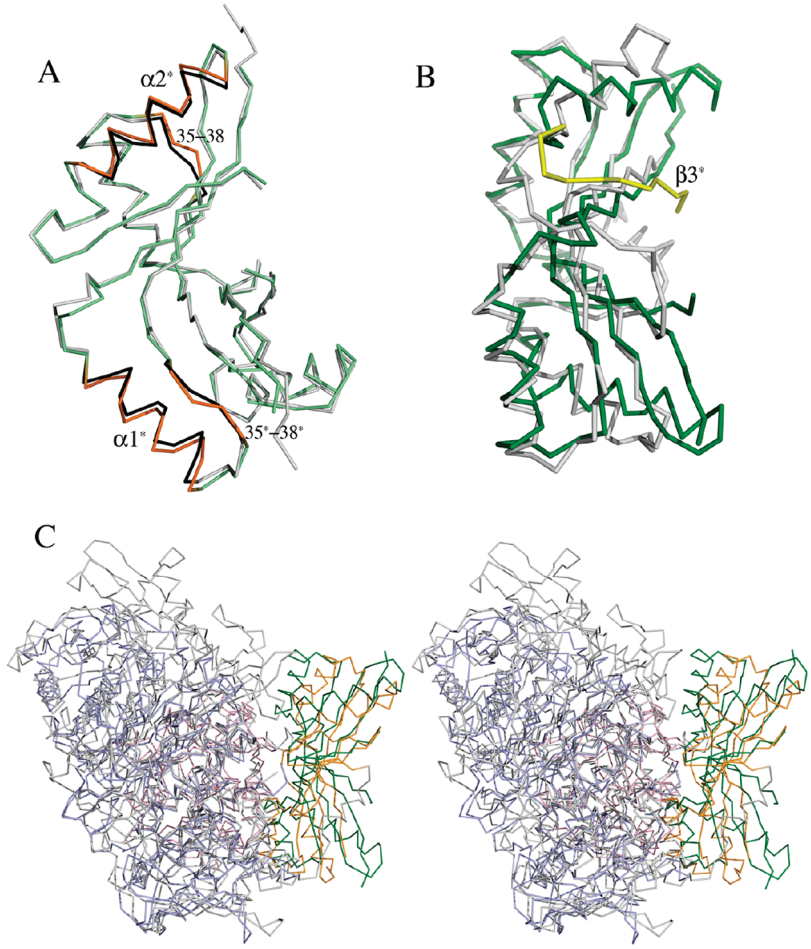

FIGURE 5: Conformational changes of TmPurS. (A) A Cα-trace of the superposition of the complexed TmPurS, in pale green, and the published TmPurS structure, in gray. The structural elements that differ between the two structures are in orange for the complexed TmPurS and in black for the native TmPurS. (B) A Cα-trace of the superposition of the complexed TmPurS, in green, with N-terminal domain of StPurL, in gray. In yellow is the additional strand found in TmPurS. (C) Stereoview of the overall superposition of TmPurLQS with StPurL in ribbon representation. TmPurS is in green; TmPurL is in pale-blue; TmPurQ is in light pink. The N-terminal domain of StPurL is in orange; the rest of StPurL is in gray.

TmPurQ. Of these structural elements, helix α31 is involved in the interaction with the FGAM synthetase domain. The active site residues are strictly conserved, and superimpose almost completely in the two structures.

Comparison of TmPurL with the FGAM Synthetase Domain of StPurL. The FGAM synthetase domain of StPurL shares 21% sequence identity with TmPurL, with an rmsd deviation of 2.6 Å^2. The FGAM synthetase domain of StPurL is a highly decorated version of TmPurL, with the core remaining the same (Figure 3C). The half of the molecule that includes the A1-B1 subdomains and the active site is more conserved structurally. The differences in this half are found in the A1 subdomain and include three elongated loops with pairs of β-strands: β6-β7, β9-β10, β14-β15. The A2 subdomain is well conserved with the loops being more elaborate for the StPurL structure, and including insertions β29-β30, and helix α17. The B2 subdomain shows the biggest differences between the two structures, with four helices and two strands deleted in TmPurL. These include helices α22 and α26, and C-terminal residues 960−1015, which include β37, β38, α27 and α28. The comparison of the domain interfaces in StPurL with the protein interfaces in TmPurLQS is included in Supporting Information (Supplemental Figure 3).

Motions of TmPurS. The TmPurS structure from the complex was compared with the reported structure of TmPurS as well as the N-terminal domain of StPurL. A structural superposition of the uncomplexed TmPurS and the complexed TmPurS reveals no significant conformational changes, with an rmsd of 0.7 Å^2. In order to look for more subtle changes, a difference distance matrix plot (DDMP) was produced using the DDMP program (*31*) from the Center for Structural Biology at Yale University, New Haven, CT. This comparison reveals that there are two structural changes associated with the complexed PurS (Figure 5A). First is a movement of a loop between α1 and β2 present in both monomers. Motion of up to 2 Å is characteristic of this region and most pronounced for residues Asn35, Lys37, and Lys38. The hydrogen-bonding pattern remains the same as in the uncomplexed structure, with the bonds being slightly longer to account for the motion. The second movement is substantial only for monomer 2 of TmPurS, which interacts with TmPurQ. Two helices α1 and α2 form a more open conformation in this monomer; the residues within the helices shift further apart, with the distance between equivalent points increasing by 1.5−1.7 Å, and the overall angle being 5° more obtuse than in the uncomplexed structure. Although the helices are not part of the complex interface, the loops

associated with both are part of the interface. Considering the low resolution of the complex, a cautious interpretation of the movement is that the complexed TmPurS is possibly less concave, as if adhering to the other two proteins to provide tighter interactions within the complex.

The N-terminal domain of StPurL shares 14% sequence identity with TmPurS. However, the dimer of TmPurS is structurally similar to this domain with an rmsd of 2.4 Å (Figure 5B). The N-terminal domain lacks one strand that corresponds to β3 of monomer 2 in TmPurS and adopts a less concave shape than TmPurS. Since the interactions between the domains in StPurL are more extensive than those between the proteins in TmPurLQS, the concavity of the PurS structure (or the N-terminal domain in large PurL) could well be related to the tightness of the interactions within the complex, with least concave being the tightest. This observation is consistent with the fact that the structure of TmPurS alone is the most concave of the three, as there are no domain interactions present. The concavity of the PurS dimer within the TmPurLQS complex, where the protein interfaces are weaker than for the corresponding domains of StPurL, falls between that of PurS alone and the PurS-like N-terminal domain of StPurL. Finally, StPurL has the tightest interfaces, and hence the least concave shape of the PurS-like N-terminal domains.

While no systematic movement of TmPurL and TmPurQ is observed upon the superposition of the complex with StPurL, TmPurS shows a change in orientation. TmPurS undergoes a rocking motion of 5°; helices α1 of monomer 2 and α2 of monomer 1 shift toward TmPurL, while α1 of monomer 1 and α2 monomer 2 shift away from TmPurL (Figure 5C). This motion points to the flexibility of the complex and the ability of PurS to assume different orientations with respect to PurQ and PurL.

Motions of TmPurL, Active Site. TmPurL from the TmPurLQS complex was compared with the six published TmPurL structures. The superpositions with these structures reveal three loop regions with a difference in Cα carbon positions greater than 5 Å; two of these regions are located in the active site and the third in the auxiliary site (Figure 6A). The flexible loop between α3 and β1 (residues 44−60), which caps the nucleotide in the active site, shows large variation, as expected in the absence of the substrates. The loop between α7 and α8 of subdomain A2, residues 203−209, is part of the region that becomes ordered upon FGAR binding. This loop moves closer to the active site in the FGAR bound structures with Gln208 forming a hydrogen bond to the formyl moiety of FGAR, while in the complex structure the loop is shifted away by approximately 3.5 Å and forms interactions with TmPurS (Figure 6B). In the complex, the carbonyl moiety of Thr203 from TmPurL is positioned to form a hydrogen bond with the side chain of Arg13 from TmPurS, and the carbonyl moiety of Lys204 from TmPurL is near the side chain of Asn15 from TmPurS. These two regions represent the largest deviation in the conformation of this loop. TmPurL structures with no FGAR or PurS bound also show a shift toward the active site; however the shift is approximately half the distance of that when FGAR is present.

Consequently, besides the encapsulation of the substrate, this region of the active site appears to take part in the modulation of the TmPurS interactions with TmPurL. The active site loop could swing out to form contacts with PurS; PurS could then be pulled closer to PurL upon FGAR binding and ordering of the remainder of the loop. This observation is consistent with the sequential order of binding described for the *E. coli* PurL system; FGAR being the last substrate to bind could trigger the formation of a tighter seal between PurL and PurS, preventing both hydrolysis of a phosphorylated FGAR-intermediate by solvent and escape of NH_3 (*19*).

Motions of TmPurL, Auxiliary Site. The most dramatic movement in the structure of TmPurL is observed for residues 360−390, which include the long linker region connecting subdomains B1 and A2 and the β12 strand of subdomain A2. This region forms a part of the auxiliary nucleotide binding site (Figure 6A). Of all available TmPurL structures, the conformation of this loop in the TmPurLQS complex is most similar to the structure with an ATP molecule bound in the auxiliary site. The binding mode of the ATP molecule itself is almost identical to the ADP (or possible ATP) binding in the TmPurLQS complex. The similarity in the protein conformation is due to a shift involving residues 360−366, observed in both structures upon nucleotide binding, which occurs to avoid steric clashes of the nucleotide with Ala366 (Figure 6C). The rest of the loop is missing in the ATP-bound structure and adopts a more flattened conformation in structures with unoccupied auxiliary sites, exemplified by the TmPurL−FGAR structure in Figure 6C, while in the TmPurLQS complex this loop is more elongated. This motion is necessary in order to avoid close contacts with the TmPurQ loop between β5 and β6, residues 103−116.

In TmPurL, a small helical segment consisting of residues 367−373 is present in all structures and retains the same hydrogen-bonding pattern; however, its orientation is different. In the uncomplexed structures, the backbone carbonyl of Phe370 forms hydrogen bonds with Gln372, Tyr373, and His375; in the complexed structure, the hydrogen bonds with Tyr373 and Gln372 appear to be maintained, but not with His375. The shift in the helical fragment and the loop that follows is as large as 8 Å, and the hydrogen-bonding network that follows Phe370 is completely different for complexed versus uncomplexed structures.

The main interactions that appear to be formed or broken at the PurL/Q interface upon the complex formation are listed. The main chain carbonyl of Glu371 appears to form a hydrogen bond with the amide of Asp374 in the uncomplexed TmPurL, and with the amide of Cys112 of TmPurQ in the complexed TmPurL structure. The hydroxyl of Tyr373 interacts with Asp116 in the unbound TmPurL, and with Asp107 in the bound TmPurL. The side chain of Asp374 does not have a hydrogen-bonding partner in the uncomplexed TmPurL, and appears to hydrogen bond to Arg189 of TmPurQ in the complex. This salt bridge is structurally conserved in StPurL. His375 interacts with Asn127 and Thr133 in unbound TmPurL, and with Tyr373 and Thr381 in the bound TmPurL. The carbonyl moiety of Thr379 in complexed TmPurL, which forms a hydrogen bond with the main chain amide of Arg393, is responsible for the shift of residues 390−395, located in a loop, closer to the long linker region. None of the linker residues in the uncomplexed TmPurL interact with this loop. Starting with residue Val382, the loop adopts the same orientation in both structures,

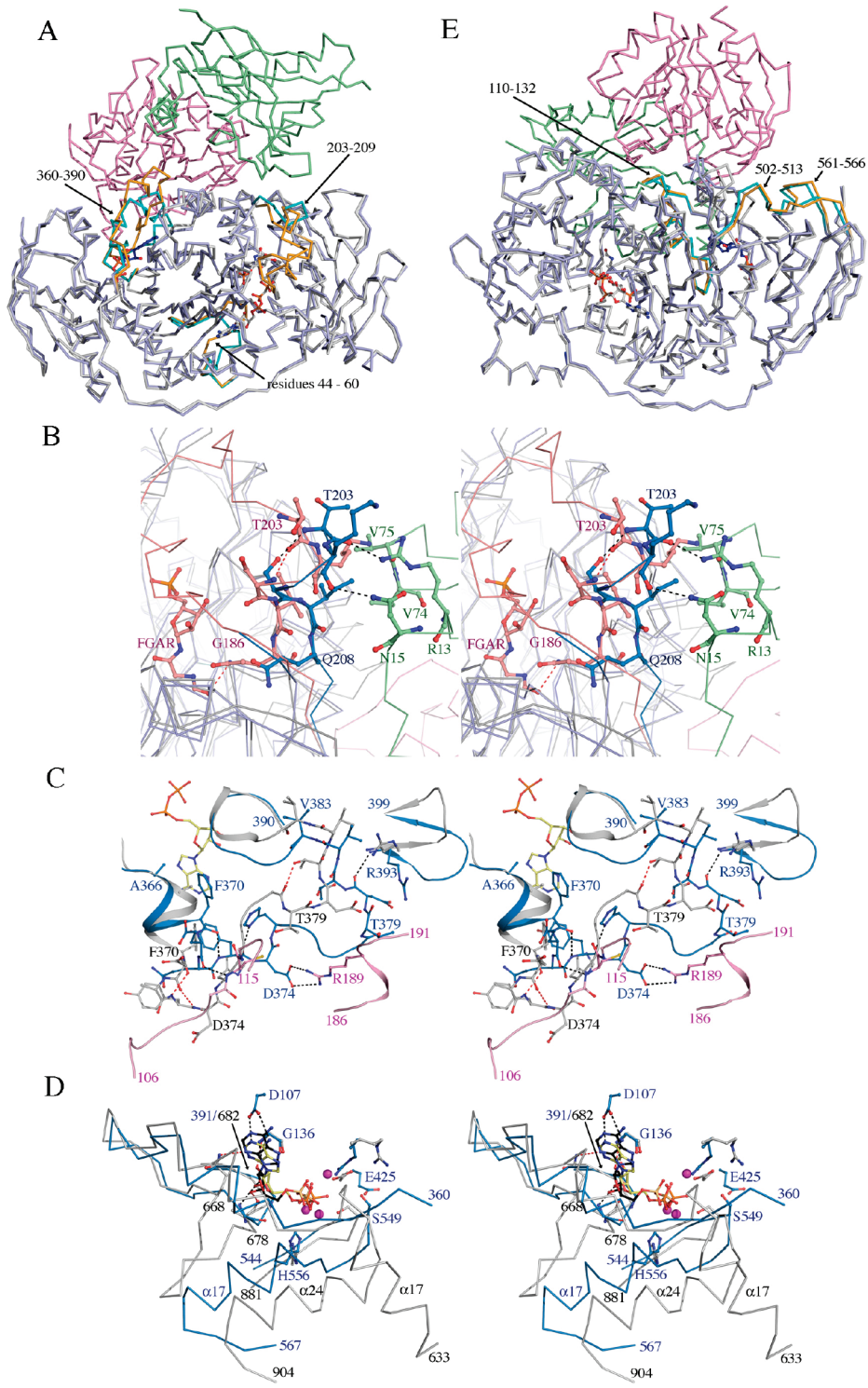

FIGURE 6: Conformational changes in TmPurL. (A) A Cα-trace of the superposition of TmPurLQS with the TmPurL/FGAR/AMPPCP complex highlighting major movements. TmPurQ is in light pink; TmPurS is in pale-green. Complexed TmPurL is in pale-blue; uncomplexed TmPurL is in gray. The structural elements that differ between the two structures are in cyan for the complexed TmPurL and in orange for the uncomplexed TmPurL. (B) Stereoview of the superposition of TmPurLQS with the TmPurL/FGAR/AMPPCP structure. TmPurS is in green; TmPurL of the TmPurLQS complex is in pale-blue; the uncomplexed TmPurL is in gray. The structural elements that differ between the two structures are in skyblue for the complexed TmPurL and in salmon for the uncomplexed TmPurL. Residues and ligands responsible for the motion are shown in ball-and-stick representation. Dotted lines are hydrogen bonds. (C) Stereoview of the superposition of TmPurLQS with the TmPurL/FGAR/AMPPCP structure. TmPurQ is in pink; TmPurL of the TmPurLQS complex is in skyblue; the uncomplexed TmPurL is in gray. Some of the residues and ligands involved in the motion are shown in ball-and-stick representation. (D) Stereoview of the superposition of the auxiliary sites of TmPurL and StPurL. In blue is TmPurL; in gray is StPurL. In ball-and-stick representation are the ligands, yellow in TmPurL and black in StPurL, and the residues structurally conserved between the two structures. Magenta spheres are the magnesium ions bound in StPurL. Residue numbering is colored blue in TmPurL, and black in StPurL. (E) Superposition of TmPurLQS with the TmPurL/FGAR/AMPPCP complex highlighting minor movements. TmPurQ is in light pink; TmPurS is in pale-green. Complexed TmPurL is in pale-blue, while uncomplexed TmPurL is in gray. The structural elements that differ between the two structures are in cyan for the complexed TmPurL and in orange for the uncomplexed TmPurL.

although the shift of 2 Å is still present and slowly diminishes by residue 389.

The location of the long linker region, which is able to obtain multiple conformations, between the auxiliary site of PurL and the TmPurL/Q interface suggests the importance of the auxiliary site in the recruitment of PurQ in the complex formation. A likely scenario is that the binding of the nucleotide in the auxiliary site triggers and stabilizes the necessary conformation of the loop. Since the loop is in the center of the PurL/Q interface and makes up a third of the protein−protein interactions, this conformation is likely crucial for recognition and docking of PurQ.

Comparison of TmPurLQS and StPurL structures reveals that the nucleotide in the auxiliary site is bound in a similar binding pocket maintaining a similar orientation in both (Figure 6D). Unlike the uncomplexed TmPurL structures, in StPurL the loop corresponding to residues 360−390 adopts the same conformation as that in the TmPurLQS complex, confirming the importance of this particular loop conformation for the complex formation. The α17 helix of StPurL has been proposed to be important for the communication between the subdomains (*9*). While this helix is missing in the TmPurL structure, its C-terminus is located in the beginning of the long B1-A2 linker region, where some of the most significant conformational changes take place upon complex formation, supporting the possibility of its role in domain communication.

The auxiliary nucleotide in StPurL is bound very tightly and cannot be removed without denaturing the protein (*9*). One interesting question is how the nucleotide becomes inserted into the auxiliary site. The region corresponding to α17 is unlikely to be the entry point of the nucleotide to the auxiliary site due to its rigidity. The entry of the nucleotide is likely to be in the region related to the active site ATP by the pseudo 2-fold axis. In StPurL, this cavity entrance is blocked by a loop insertion of residues 668−677, which interacts with helix α24 (α17 of TmPurL), and further blocked off by the glutaminase domain, making the nucleotide structural in StPurL and likely inserted during protein folding. In TmPurL, however, this helix is adjacent to and interacts intimately with the large flexible loop of 360−390; thus, unless TmPurQ is bound to TmPurL, and the large loop is rigid, the nucleotide can easily diffuse in and out of the auxiliary site, supporting a mechanism where binding of the nucleotide in the auxiliary site triggers conformational changes in a large flexible region and is then followed by recruitment of TmPurQ.

While the secondary structure of the auxiliary site is conserved between TmPurL and StPurL, there is very little conservation in the primary structure. Of the 25 residues involved in the interaction with the nucleotide, four are structurally conserved: Glu425, Gly136, Ser549, and Arg139 (Glu718, Gly387, Ser886, Arg390 in StPurL). All but Gly136 are involved in coordination of the phosphate tail. The similarity between the two sites is mostly in the ribose being bound via main chain atoms and the hydrophobic pocket for the adenine base being conserved functionally. It remains unclear whether the auxiliary nucleotide binding in TmPurLQS complex has any additional function other than structural facilitation of complex formation via ordering of the 360−390 loop region, and whether or not ATP and ADP are functionally equivalent for this purpose, given that the enzyme activity is not inhibited by the presence of PK/PEP, as was previously observed for BsPurLQS (*15*).

Motions of TmPurL, Concerted Subdomain Movements. To observe more subtle differences in the TmPurL structures, DDMPs were produced and reveal the differences with a minimum of 1 Å and a maximum of 5 Å shift. Most similar to the complexed TmPurLQS structure is the TmPurL−ATP/ATP structure (Supplemental Figure 4A, Supporting Information). No significant systematic movement occurs within each of the four individual subdomains of TmPurL, except for small movements of the loop regions between β8 and α11 (subdomain B1) and between β15 and β16 (subdomain A2), probably due to general loop flexibility. Little change is also seen upon comparison with the TmPurL/ADP structure, suggesting that binding of the nucleotides in the active and auxiliary sites does not affect the overall subdomain conformation.

Unliganded TmPurL shows some variation when compared to the TmPurLSQ complex. While there are no significant shifts within the two halves of the molecule (A1 does not move with respect to B1, and A2 does not move with respect to B2), they show small systematic movement with respect to each other. A2 subdomain appears to shift away from the active site half of the molecule, while B2 appears to shift closer. These movements, which are not uniform and appear in patches of residues, become even more pronounced upon comparison with the two FGAR bound structures (Supplemental Figure 4B). The patches mainly comprise loop regions, and there are three such patches in A2 and four in B2. Three of the regions are part of the TmPurL/Q interface. The linker between A2 and B2 (residues 502−513), and the turn between α17 and β19 (residues 561−566) from B2 subdomain move uniformly closer to the A1-B1 half of the molecule (Figure 6E). Residues 110−132 of A1, also part of the TmPurL/TmPurQ interface, shift uniformly closer to the B2 subdomain. In summary, the A1-B1 half of the molecule shows less movement than the A2-B2 half, with the tendency of the auxiliary cleft to become narrower upon FGAR binding.

These subtle subdomain shifts indicate the possibility of communication between the active and auxiliary sites. FGAR could act as the trigger for complex activation, securing PurS as described above and causing shifts in the auxiliary site as indicated by the subtle subdomain movements. The auxiliary site, which interacts with PurQ, would in turn propagate the signal to the PurQ/L interface, securing this part of the complex and triggering glutaminase activity.

Ammonia Channel. Two possibilities for an ammonia channel have been proposed for StPurL. Upon examination of the TmPurLQS complex structure, similar possibilities are revealed (Figure 7A); however, only one channel shows a high degree of conservation. For both channels, ammonia would leave the TmPurQ active site at the same exit point that consists of the two phenylalanines, 51 and 110. Ammonia could then pass through to either side of helices α5 and α6 of subdomain A1. One channel, labeled channel A in Figure 7A, runs along the side of the β-barrel, the auxiliary site and into the active site. Channel B in Figure 7A is located on the other side of the helices and consists of the point where the interfaces of all three proteins meet, the loop between β1 and α1 of TmPurS monomer 1, and the loop consisting of residues 203−210 of TmPurL, which shows

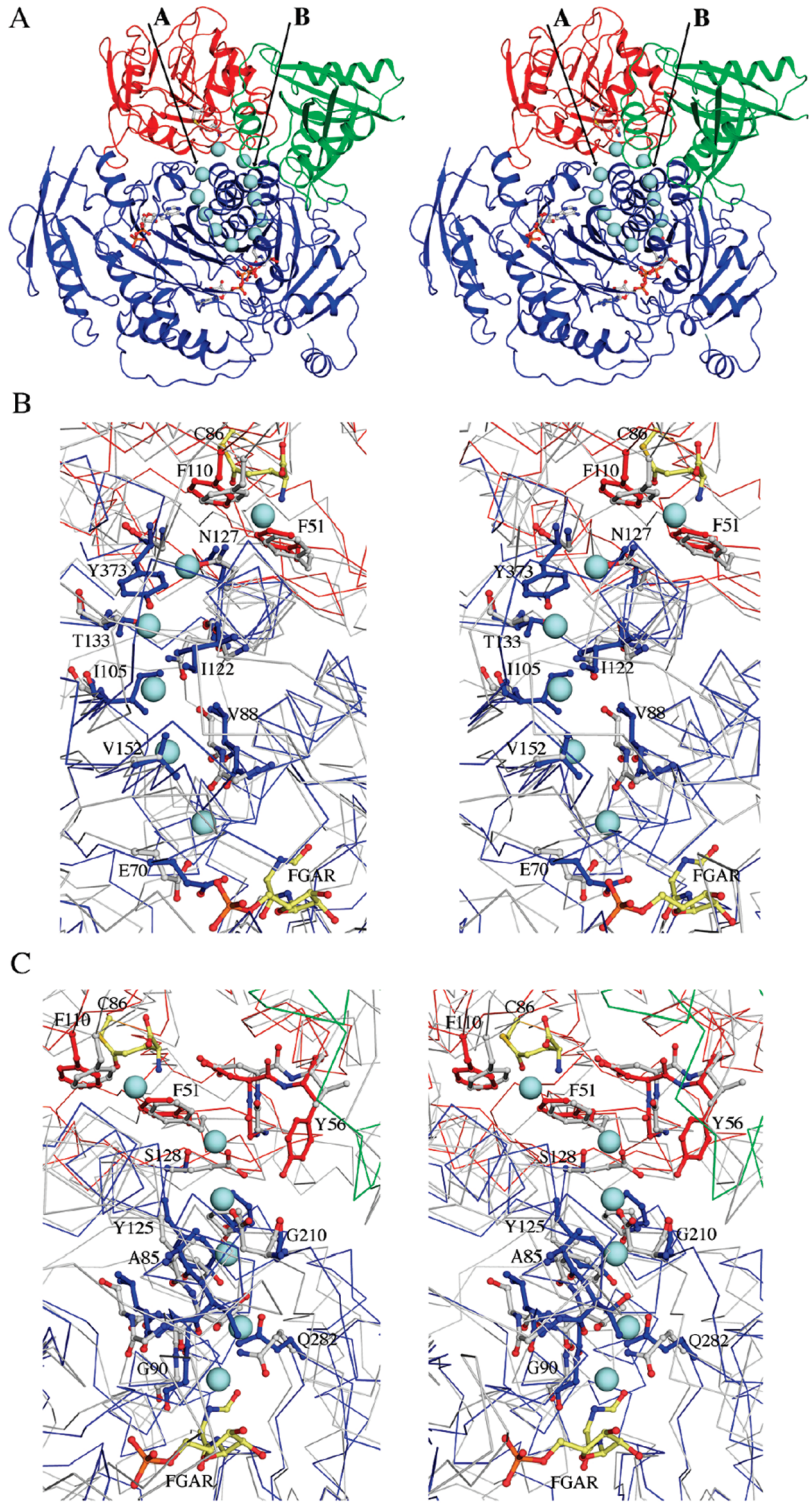

FIGURE 7: Ammonia channel in TmPurLQS. (A) Stereoview of the TmPurLQS as a ribbon diagram. TmPurS is in green, TmPurQ is in red, TmPurL is in blue. Ligands modeled in the active and auxiliary sites are shown in ball-and-stick. The light blue spheres mark the two possible paths for ammonia, labeled A and B. (B) Stereoview of the superposition of channel A from TmPurL with StPurL. Color-coding of TmPurLQS is the same as in panel A; StPurL is in gray. Residues lining the channel are in ball-and-stick. The residue numbering in black is for TmPurLQS. (C) Stereoview of the superposition of channel B from TmPurL with StPurL. Color-coding and labeling are the same as in panel B.

conformational variation depending on substrate binding and complex formation, and the rest of the active site of TmPurL.

Comparison of the StPurL structure with the TmPurLQS complex structure reveals that channel A contains five bulky substitutions in the TmPurL structure (Figure 7B). In StPurL, residues Gly331, Gly373, Ala384, Ala414, and Gly656, which line this proposed ammonia path, are replaced by Ile105, Ile122, Thr133, Val152 and Tyr373, respectively. Channel B on the other hand contains structurally conserved residues: Gly54, Glu55 from TmPurQ, and Ala85, Thr86, Gly87, Gly89, Gly90, Pro212, and Gln282 from TmPurL. Moreover, all of these residues except Ala85 are strictly conserved based on the sequence alignments of large and small PurLs. The substitutions that are found in this channel

are either conservative, such as Tyr125 changed to a Phe in StPurL, or for a less bulky residue, such as Gly210 changed to an Asp in StPurL. While Tyr125 or Phe are strictly conserved among all PurL sequences, this is not the case for Gly210. This residue is conserved among small PurLs, but Asp found in StPurL is not conserved among large PurLs. The location of channel B at the interface of the three proteins, and near the regulatory loop, 200−210, as well as its structural conservation, all suggest that this is the more likely path for the ammonia.

Summary of the Mechanistic Implications for the Complex Formation. From the comparisons presented above, the following mechanism for the complex formation and catalytic activation can be envisioned. The PurL structure is flexible, with conformational changes observed on various levels, subtle shifts in subdomains, and large movements in secondary structural elements. Both the active and the auxiliary site cavities appear to play a role in the complex assembly. The loop of the empty active site recruits PurS by swinging out into the solvent, while binding of a nucleotide in the auxiliary site makes the docking of PurQ possible. Even though a crystal structure of isolated PurQ in the absence of glutamine has not yet been obtained, it is likely, based on our observations by size-exclusion chromatography in both BsPurLQS (*15*) and TmPurLQS, that a PurQ−glutamine or PurQ−glutamylthioester complex is important for this docking interaction. Catalytic activation of the complex occurs during FGAR binding. It secures and possibly activates PurQ by triggering the narrowing of the auxiliary cleft with a bound nucleotide, and pulls PurS closer over the active site via ordering of the remainder of the active site loop. The rocking and bending motions observed for TmPurS show that it contains the flexibility necessary for such facilitation of the PurL−PurQ interactions. The proposed ammonia channel is located at the interface of the TmPurL active site loop and TmPurS. Hence, PurS could also facilitate the formation of the ammonia channel in the presence of FGAR and the coupling of catalysis between the two active sites. While the purpose of this mechanism is to propose a possible course of events in protein−protein interactions and complex formation on atomic level, further studies are necessary for its confirmation.

ACKNOWLEDGMENT

We thank Leslie Kinsland for assistance in the preparation of the manuscript. We thank the NE-CAT staff at beamline 24-ID-C of the Advanced Photon Source for assistance with data collection. The Cornell Protein Production and Characterization Facility is gratefully acknowledged.

SUPPORTING INFORMATION AVAILABLE

A table of primers used in TmPurL cloning, a table of potential hydrogen bonds at the TmPurLQS protein−protein interfaces, gel filtration chromatograms and the SDS gel corresponding to the TmPurLQS elution peak, a figure and topology diagram for TmPurS, a figure comparing the interfaces in TmPurLQS and StPurL, and a figure comparing the domain and subdomain movements. This material is available free of charge via the Internet at http://pubs.acs.org.

REFERENCES

1. Hyde, C. C., Ahmed, S. A., Padlan, E. A., Miles, E. W., and Davies, D. R. (1988) Three-dimensional structure of the tryptophan synthase $\alpha_2\beta_2$ multienzyme complex from *Salmonella typhimurium*. *J. Biol. Chem. 263*, 17857–17871.
2. Raushel, F. M., Thoden, J. B., and Holden, H. M. (2003) Enzymes with molecular tunnels. *Acc. Chem. Res. 36*, 539–548.
3. Weeks, A., Lund, L., and Raushel, F. M. (2006) Tunneling of intermediates in enzyme-catalyzed reactions. *Curr. Opin. Chem. Biol. 10*, 465–472.
4. Cramer, P., Bushnell, D. A., and Kornberg, R. D. (2001) Structural basis of transcription: RNA polymerase II at 2.8 Å resolution. *Science 292*, 1863–1876.
5. Leibundgut, M., Jenni, S., Frick, C., and Ban, N. (2007) Structural basis for substrate delivery by acyl carrier protein in the yeast fatty acid synthase. *Science 316*, 288–290.
6. Mouilleron, S., and Golinelli-Pimpaneau, B. (2007) Conformational changes in ammonia-channeling glutamine amidotransferases. *Curr. Opin. Struct. Biol. 17*, 653–664.
7. Levenberg, B., Hartman, S. C., and Buchanan, J. M. (1956) Biosynthesis of the purines. X. Further studies *in vitro* on the metabolic origin of nitrogen atoms 1 and 3 of the purine ring. *J. Biol. Chem. 220*, 379–390.
8. Melnick, I., and Buchanan, J. M. (1957) Biosynthesis of the purines. XIV. Conversion of (α-N-formyl) glycinamide ribotide to (α-N-formyl) glycinamidine ribotide; purification and requirements of the enzyme system. *J. Biol. Chem. 225*, 157–162.
9. Anand, R., Hoskins, A. A., Stubbe, J., and Ealick, S. E. (2004) Domain organization of *Salmonella typhimurium* formylglycinamide ribonucleotide amidotransferase revealed by X-ray crystallography, *Biochemistry 43*, 10328–10342.
10. Mathews, I. I., Krishna, S. S., Schwarzenbacher, R., McMullan, D., Abdubek, P., Ambing, E., Canaves, J. M., Chiu, H. J., Deacon, A. M., DiDonato, M., Elsliger, M. A., Godzik, A., Grittini, C., Grzechnik, S. K., Hale, J., Hampton, E., Han, G. W., Haugen, J., Jaroszewski, L., Klock, H. E., Koesema, E., Kreusch, A., Kuhn, P., Lesley, S. A., Levin, I., Miller, M. D., Moy, K., Nigoghossian, E., Paulsen, J., Quijano, K., Reyes, R., Spraggon, G., Stevens, R. C., vandenBedem, H., Velasquez, J., White, A., Wolf, G., Xu, Q., Hodgson, K. O., Wooley, J., and Wilson, I. A. (2006) Crystal structure of phosphoribosylformylglycinamidine synthase II (smPurL) from *Thermotoga maritima* at 2.15 Å resolution. *Proteins 63*, 1106–1111.
11. Morar, M., Anand, R., Hoskins, A. A., Stubbe, J., and Ealick, S. E. (2006) Complexed structures of formylglycinamide ribonucleotide amidotransferase from *Thermotoga maritima* describe a novel ATP binding protein superfamily. *Biochemistry 45*, 14880–14895.
12. Anand, R., Hoskins, A. A., Bennett, E. M., Sintchak, M. D., Stubbe, J., and Ealick, S. E. (2004) A model for the *Bacillus subtilis* formylglycinamide ribonucleotide amidotransferase multiprotein complex. *Biochemistry 43*, 10343–10352.
13. Batra, R., Christendat, D., Edwards, A., Arrowsmith, C., and Tong, L. (2002) Crystal structure of MTH169, a crucial component of phosphoribosylformylglycinamidine synthetase. *Proteins 49*, 285–288.
14. Mathews, I. I., Krishna, S. S., Schwarzenbacher, R., McMullan, D., Jaroszewski, L., Miller, M. D., Abdubek, P., Agarwalla, S., Ambing, E., Axelrod, H. L., Canaves, J. M., Carlton, D., Chiu, H. J., Clayton, T., DiDonato, M., Duan, L., Elsliger, M. A., Grzechnik, S. K., Hale, J., Hampton, E., Haugen, J., Jin, K. K., Klock, H. E., Koesema, E., Kovarik, J. S., Kreusch, A., Kuhn, P., Levin, I., Morse, A. T., Nigoghossian, E., Okach, L., Oommachen, S., Paulsen, J., Quijano, K., Reyes, R., Rife, C. L., Spraggon, G., Stevens, R. C., van den Bedem, H., White, A., Wolf, G., Xu, Q., Hodgson, K. O., Wooley, J., Deacon, A. M., Godzik, A., Lesley, S. A., and Wilson, I. A. (2006) Crystal structure of phosphoribosylformyl-glycinamidine synthase II, PurS subunit (TM1244) from *Thermotoga maritima* at 1.90 Å resolution. *Proteins 65*, 249–254.
15. Hoskins, A. A., Anand, R., Ealick, S. E., and Stubbe, J. (2004) The formylglycinamide ribonucleotide amidotransferase complex from *Bacillus subtilis*: metabolite-mediated complex formation. *Biochemistry 43*, 10314–10327.
16. Thoden, J. B., Huang, X., Raushel, F. M., and Holden, H. M. (1999) The small subunit of carbamoyl phosphate synthetase: snapshots along the reaction pathway. *Biochemistry 38*, 16158–16166.
17. Buchanan, J. M. (1982) Covalent reaction of substrates and antimetabolites with formylglycinamide ribonucleotide amidotransferase. *Methods Enzymol. 87*, 76–84.
18. Satterthwait, A. C., and Westheimer, F. H. (1980) Monomeric methyl metaphosphate: reactions with carbonyl groups. *J. Am. Chem. Soc. 102*, 4464–4472.

19. Schendel, F. J., Mueller, E., Stubbe, J., Shiau, A., and Smith, J. M. (1989) Formylglycinamide ribonucleotide synthetase from *Escherichia coli*: cloning, sequencing, overproduction, isolation, and characterization. *Biochemistry 28*, 2459–2471.
20. Otwinowski, Z., and Minor, W. (1997) Processing of X-ray diffraction data collected in oscillation mode. *Methods Enzymol. 276*, 307–326.
21. Collaborative Computational Project-Number 4 (1994) The CCP-4 suite: programs for protein crystallography. *Acta Crystallogr. D 50*, 760−763.
22. Brünger, A. T., Adams, P. D., Clore, G. M., DeLano, W. L., Gros, P., Grosse-Kunstleve, R. W., Jiang, J. S., Kuszewski, J., Nilges, M., Pannu, N. S., Read, R. J., Rice, L. M., Simonson, T., and Warren, G. L. (1998) Crystallography & NMR system: A new software suite for macromolecular structure determination. *Acta Crystallogr. D 54*, 905–921.
23. Emsley, P., and Cowtan, K. (2004) Coot: model-building tools for molecular graphics. *Acta Crystallogr. D 60*, 2126–2132.
24. Kleywegt, G. J., and Jones, T. A. (1996) xdlMAPMAN and xdlDATAMAN-programs for reformatting, analysis, and manipulation of biomacromolecular electron-density maps and reflection datasets. *Acta Crystallogr. D 52*, 826–828.
25. DeLano, W. L. (2002) *The PyMOL Molecular Graphics Systems*, Delano Publishing, San Carlos, CA.
26. Hoskins, A. A. (2006) *Channeling in Purine Biosynthesis: Efforts to Detect Interactions Between PurF and PurD and Characterization of the FGAR-AT Complex*, Ph.D. Thesis, Massachusetts Institute of Technology, Cambridge, MA.
27. Laskowski, R. A., MacArthur, M. W., Moss, D. S., and Thornton, J. M. (1993) PROCHECK: a program to check the stereochemical quality of protein structures. *J. Appl. Crystallogr. 26*, 283–291.
28. Goto, M., Omi, R., Nakagawa, N., Miyahara, I., and Hirotsu, K. (2004) Crystal structures of CTP synthetase reveal ATP, UTP, and glutamine binding sites. *Structure 12*, 1413–1423.
29. Raushel, F. M., Thoden, J. B., and Holden, H. M. (1999) The amidotransferase family of enzymes: molecular machines for the production and delivery of ammonia. *Biochemistry 38*, 7891–7899.
30. Spraggon, G., Kim, C., Nguyen-Huu, X., Yee, M. C., Yanofsky, C., and Mills, S. E. (2001) The structures of anthranilate synthase of Serratia marcescens crystallized in the presence of (i) its substrates, chorismate and glutamine, and a product, glutamate, and (ii) its end-product inhibitor, L-tryptophan. *Proc. Natl. Acad. Sci. U.S.A. 98*, 6021–6026.
31. Richards, F. M., and Kundrot, C. E. (1988) Identification of structural motifs from protein coordinate data: secondary structure and first-level supersecondary structure. *Proteins 3*, 71–84.

BI800329P